MIT Libraries | DSpace@MIT

MIT Open Access Articles

Ultrathin Conformal oCVD PEDOT Coatings on Carbon Electrodes Enable Improved Performance of Redox Flow Batteries

The MIT Faculty has made this article openly available. ***Please share*** how this access benefits you. Your story matters.

Citation: Heydari Gharahcheshmeh, Meysam, Wan, Charles Tai#Chieh, Ashraf Gandomi, Yasser, Greco, Katharine V., Forner#Cuenca, Antoni et al. 2020. "Ultrathin Conformal oCVD PEDOT Coatings on Carbon Electrodes Enable Improved Performance of Redox Flow Batteries." Advanced Materials Interfaces, 7 (20).

As Published: http://dx.doi.org/10.1002/admi.202000855

Publisher: Wiley

Persistent URL: https://hdl.handle.net/1721.1/140512

Version: Author's final manuscript: final author's manuscript post peer review, without publisher's formatting or copy editing

Terms of use: Creative Commons Attribution-Noncommercial-Share Alike

Massachusetts Institute of Technology

Check for updates

Ultrathin Conformal oCVD PEDOT Coatings on Carbon Electrodes Enable Improved Performance of Redox Flow Batteries

Meysam Heydari Gharahcheshmeh[1,*], Charles Tai-Chieh Wan[1,*], Yasser Ashraf Gandomi[1], Katharine Greco[1], Antoni Forner-Cuenca[1], Yet-Ming Chiang[2], Fikile R. Brushett[1,†], Karen K. Gleason[1,†]

[1] Department of Chemical Engineering, Massachusetts Institute of Technology, 77 Massachusetts Avenue, Cambridge, MA 02139, United States

[2] Department of Materials Science and Engineering, Massachusetts Institute of Technology, 77 Massachusetts Avenue, Cambridge, MA 02139, United States

[*] These authors contributed equally to this work

[†] Corresponding Authors: Email: brushett@mit.edu (F.R.B); kkgleasn@mit.edu (K.K.G.)

Author Manuscript

Abstract

Surface engineering of porous carbon electrodes is an effective strategy to enhance power output of redox flow batteries (RFBs) and may enable new cost reduction pathways for energy storage. Here, we demonstrate a surface modification strategy that enhances the electrochemical performance of RFBs in iron-based electrolytes. We conformally grow nanometric films of poly(3,4-ethylene dioxythiophene) (PEDOT) onto carbon cloth electrodes using oxidative chemical vapor deposition (oCVD) and investigate the impact of film properties on electrode performance in model iron-based electrolytes. We find that depositing oCVD PEDOT films on the electrode surface reduces ohmic, kinetic, and mass transport resistances with the highest current densities and lowest resistances observed for electrodes coated with a ~78 nm thick film. As compared to unmodified electrodes, coated electrodes enhance the maximum obtained current density at an applied overpotential of 350 mV by 6.7× and 3.7× in iron sulfate and iron chloride, respectively. The oCVD PEDOT film described here represents an initial step towards electrode surfaces of tailored activity, selectivity, and wettability for specific RFB chemistries and, more generally, electrochemical systems with liquid-phase reactants.

This is the author manuscript accepted for publication and has undergone full peer review but has not been through the copyediting, typesetting, pagination and proofreading process, which may lead to differences between this version and the Version of Record. Please cite this article as doi: 10.1002/admi.202000855.

This article is protected by copyright. All rights reserved.

Table of Content (TOC):

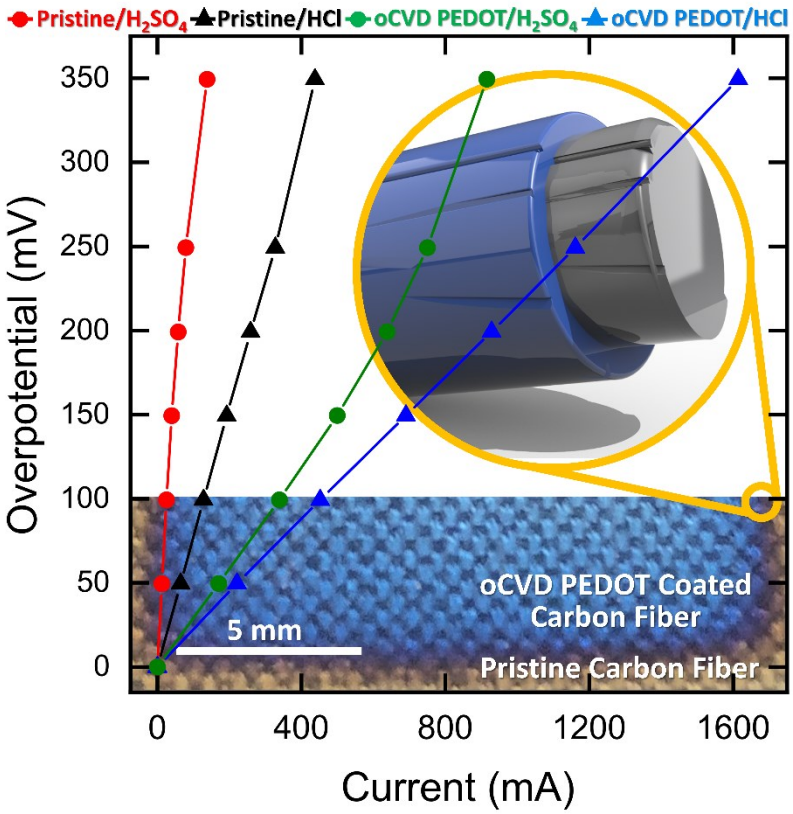

Surface engineering of porous carbon electrodes through conformal growth of nanometric PEDOT thin films using oxidative chemical vapor deposition (oCVD) is a promising approach to enhance power output of redox flow batteries. As compared to the pristine, oCVD PEDOT-coated electrodes enhance maximum current density at an applied overpotential of 350 mV by ~6.7× and ~3.7× in iron-sulfate and iron-chloride, respectively.

Keywords: oxidative chemical vapor deposition, poly(3,4-ethylenedioxythiophene), redox flow batteries

Introduction

Stationary energy storage is poised to play an instrumental role in efficiently delivering electricity, particularly from low-cost, sustainable, and variable energy sources. Redox flow batteries (RFBs) have emerged as an appealing electrochemical technology for long duration energy storage, owing to their decoupling of energy and power scaling, safety, and long operational lifetimes.[1-5] However, existing RFBs are still too expensive for broad adoption, motivating research into optimizing reactor design, electrolyte formulations, and separation strategies.

The porous carbon electrode is a critical component of the RFB stack, providing active sites for redox reactions, controlling electrolyte distribution and pressure drop, and cushioning compressive

This article is protected by copyright. All rights reserved.

Author Manuscript

forces required to seal the system and minimize contact resistances.[6] While functional, the electrodes used in advanced RFBs, which are typically based on porous carbon and graphite papers, cloths, or felts, generally possess low surface area (ca. 0.1 – 10 m^2 g^{-1}), spatially-varying surface chemistry, and poor aqueous wettability.[7] To address these limitations, electrodes are commonly oxidatively pretreated, via thermal,[8-11] electrochemical,[12] or chemical means,[13,14] which can simultaneously increase surface area and introduce oxygen-rich functionalities on the electrode surface that improve wetting and reaction kinetics. While effective, these methods offer limited control of specific surface chemistry and compositional uniformity across the three-dimensional geometry.

A potentially effective strategy for tailoring electrode-electrolyte interfaces is through the deposition of conductive polymeric overlayers, which have been shown to enhance the areal energy and power density by improving pseudocapacitance in supercapacitors[15] and stabilize the structure and thermal stability of the electrode-electrolyte interface in lithium-ion batteries with nickel-rich positive electrodes.[16] These studies utilized continuous polymer layers, as thin as 3 nm, grown by oxidative chemical vapor deposition (oCVD) to support facile electrical and ionic conduction. In contrast to solution-applied layers, the oCVD films conformally encapsulated the nanostructured surfaces, leaving void space to enable changes in polymer layer thickness upon ion-exchange without the development of significant mechanical strain. Additionally, conformal coverage maintains high surface area for effective contact with the electrolyte.

Here, we explore the potential of oCVD processing to improve the performance of carbon-fiber based electrodes in aqueous RFBs. We leverage poly(3,4-ethylenedioxythiophene (PEDOT), which is the most extensively studied oCVD polymer to date.[17-27] The oCVD approach provides remarkable capabilities for nanoscale control of thickness and crystallographic texture.[27-31] The composition and properties of oCVD PEDOT are distinct from spin-applied PEDOT:PSS (polystyrene sulfonate). In this work, the dopant species for the oCVD PEDOT is the small anion, Cl^-, whose greater mobility than PSS has been shown promotes ion-exchange in the film resulting in electrochemical activity.[30] Additionally, the electrical conductivity of oCVD PEDOT can exceed 6000 S/cm[29], several orders of magnitude higher than pristine PEDOT:PSS. Previous work demonstrated the ability to grow ultrathin, durable, and conformal PEDOT layers over the geometrically complex carbon cloth surfaces.[20]

In this work, we evaluate oCVD PEDOT modified carbon cloth electrodes in electrolytes utilized in RFBs. We employ a comprehensive set of spectroscopic techniques to assess the morphological, chemical, and structural characteristics of the oCVD PEDOT films. Using cyclic voltammetry, we show that the PEDOT coated electrode is electrochemically active in quiescent iron electrolytes containing both chloride and sulfate supporting salts. In a single-electrolyte diagnostic flow cell, we then examine the performance of oCVD PEDOT modified electrodes using polarization and assess sources of overpotential losses via impedance spectroscopy, revealing that PEDOT films mitigate ohmic, kinetic, and mass transport losses. By varying the thickness, we identify that mass transport through the film is dependent on both flow rate and thickness; we further study the role of mass transfer by varying electrolyte concentration in iron chloride electrolyte. Ultimately, we seek to demonstrate the potential of oCVD processes in tuning the performance of porous carbon electrodes and inspire the contemplation of new chemistries to address acute needs in specific electrochemical systems.

Results and Discussion

Author Manuscript

This article is protected by copyright. All rights reserved.

A conceptual image of PEDOT thin film deposition by the oCVD method is shown in **Figure 1**a. The monomer (EDOT) and oxidant ($VOCl_3$) species are introduced into a hot-wall vacuum reactor and strike on the surface of the temperature-controlled substrate through the vapor phase. The polymerization of conducting polymer in the oCVD method proceeds through the step-growth mechanism and the increase in molecular weight occurs geometrically through the formation of dimers, tetramers, and high 2N-mers.[17,32] Here, the growth temperature and film thickness of PEDOT, at the fixed monomer and oxidant flow rates into the reactor, are the primary variables for synthesizing and tuning oCVD PEDOT film properties. The experimental details related to process conditions are provided in the Supporting Information. Experimental details and information related to the equilibrium surface concentration of the reactants, determined from the saturation ratio (P/P_{sat}, where P and P_{sat} are partial pressure and saturation pressure, respectively), are provided in Table S1 (Supporting Information).

The morphology of pristine, oCVD-coated PEDOT, and spin-coated PEDOT:PSS carbon cloth electrodes are shown in **Figure 1**b-d. Carbon cloth electrodes (specifically untreated AvCarb 1071) were chosen as model porous carbon electrodes for this study due to their well-defined bimodal and binder-less woven structure, thus avoiding extraneous factors in subsequent analysis of oCVD PEDOT-coatings. The uncoated carbon fibers are ~8 μm fibers in diameter (**Figure 1**b). As predicted, the vapor deposition of PEDOT via oCVD yields uniform and highly conformal coating that retains the fibrillar nature of the carbon fibers (**Figure 1**c). However, the spun-cast PEDOT:PSS coated carbon fibers (**Figure 1**d) exhibits disadvantages, including liquid bridging, non-conformality, and delamination. In contrast to the spin-coated method, the formation of conformal coating by the oCVD method on any porous and non-planar surfaces is due to the absence of surface tension effects such as liquid-thinning, air gap formation, bridging, and meniscus formation.[17,18]

Author Manuscript

This article is protected by copyright. All rights reserved.

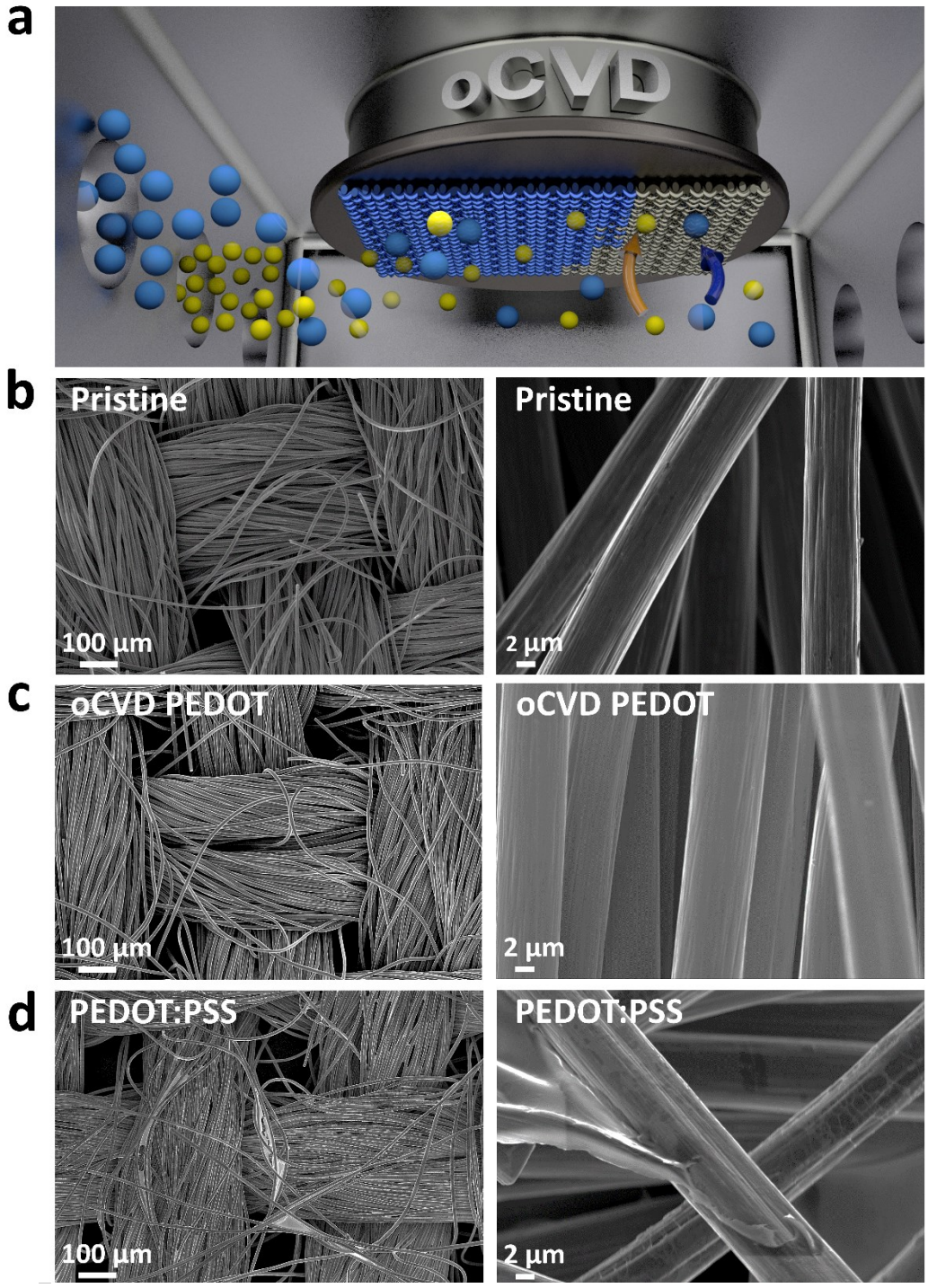

Figure 1. Schematic illustration of the oCVD method that provides ultrathin highly conformal PEDOT film on porous substrates. (a) The vapors of monomer (EDOT) and oxidant ($VOCl_3$), shown with blue and yellow-colored balls, insert into the hot-wall oCVD reactor and react spontaneously on a heated substrate in a step-growth fashion to form a conducting PEDOT thin film on the micrometric fibers of the carbon cloth electrode. The plan-view SEM images with low (left section) and high (right section) magnification for (b) blank (pristine), (c) oCVD PEDOT coated, and (d) spun-cast PEDOT:PSS coated carbon electrode.

Figure 2a further demonstrates the high conformality of oCVD PEDOT on carbon fibers via cross-sectional scanning electron microscopy (SEM) images; additional micrographs displaying the

This article is protected by copyright. All rights reserved.

conformality of the coatings on porous carbon fibers can be found in Figure S1 of the Supporting Information. The oCVD method also provides remarkable capabilities for control of conformal PEDOT thickness in various porous structures.[17,18,30] The thickness of conformally coated oCVD PEDOT thin films and penetration depth of reactants throughout the mesh electrode thickness can be adjusted by tuning the saturation ratio of oxidant and monomer. The aspect ratio (height/width ratio) in the case of carbon cloth electrode can be estimated by dividing the half-thickness of carbon cloth to the average characteristics length of spacing between fibers ($\sim \frac{1/2\ (0.38\ mm)}{12\ \mu m} \cong 16$). The half-thickness of carbon cloth is considered as a consequence of the availability of the reactants vapor species on both sides of carbon cloth due to (i) presence of a gap between heated substrate and sample, (ii) existence of large void space between each carbon bundle with the average size of ~85 μm, and (iii) constitution of cloth thickness with upper and lower wounded bundles. While measuring the penetration depth directly on the carbon cloth is experimentally challenging, the penetration depth can be estimated from measurements taken on more controlled geometries such as trench wafers. Recently, the conformality of oCVD PEDOT thin film grown with the volatile oxidant, such as $VOCl_3$, on the trench wafer with the aspect ratio of ~11 (height and width of 7.5 and 0.7 μm, respectively) is demonstrated.[27] It is noteworthy to mention that a high degree of penetration would be expected in the case of porous structure. A high degree of penetration and deposition of ultrathin conformal oCVD PEDOT film is reported in aligned carbon nanotubes (A-CNTs) with an extremely high aspect ratio of 10,000.[33]

Achieving conformal PEDOT coating by oCVD method has two significant advantages compared to the PEDOT:PSS solution-applied process in electrochemical applications; (i) maintaining a high surface area for effective contact with the electrolyte, and (ii) enabling changes in polymer thickness upon ion-exchange without the development of significant mechanical strain by leaving void space open throughout the mesh electrode thickness.[34] In addition, the oCVD PEDOT has another significant advantage over its PEDOT:PSS counterpart in electrochemical applications, due to its unique doping process. The small anion dopant, here chloride (Cl^-), makes oCVD PEDOT films compositionally distinct from spun-cast PEDOT:PSS. The small anion dopants of oCVD PEDOT more readily undergo redox exchange than the large macromolecular dopant of PSS, bringing an advantage in electrochemical applications compared to PEDOT:PSS.[17,30,35] The Raman analyses (Figure S2, Supporting Information) and attenuated total reflection-Fourier transform infrared (ATR-FTIR) spectroscopy (Figure S3, Supporting Information) confirm the polymerization and no significant structural bond changes in oCVD PEDOT films grown at different process conditions. Therefore, the texture and nanostructure of PEDOT films govern the electrical conductivity, which is in consonance with previous studies.[27-29]

The grazing incidence X-ray diffraction (GIXRD) patterns reveal that the resulting oCVD PEDOT films, grown on silicon wafers as reference samples, have an excellent ordered structure with different preferential semi-crystalline orientation (**Figure 2**b-c). The diffraction of (100) and (020) planes at 2θ values of ca. 6.4° and 25.5° correspond to the edge-on and face-on orientations, respectively. The conjugated backbone is parallel to the surface substrate in both orientations and the only difference is related to the orientation of the π-π interchain stacking, which is perpendicular and parallel to the surface substrate in face-on and edge-on orientation, respectively.

The extracted a-axis and b-axis lattice parameters were in the range of 13.80-13.84 Å and 6.97-6.99 Å, respectively. Lorentz Polarization (LP) factor, defined as: $LP(\theta) = \frac{1+cos^2(2\theta)}{sin^2(\theta)\ cos\ (\theta)}$,[27,36] was

This article is protected by copyright. All rights reserved.

Manuscript

used to quantify the percentage of preferential orientation (Table S2, Supporting Information). The change in crystallization orientation, as a function of growth temperature and film thickness, is attributed to the intermolecular interaction and energy minimization of growing film and interfaces. The obtained in-plane electrical conductivity of these samples with different preferential orientations are shown in Table S2 (Supporting Information) with higher conductivities observed for films with greater fractions of face-on orientation.

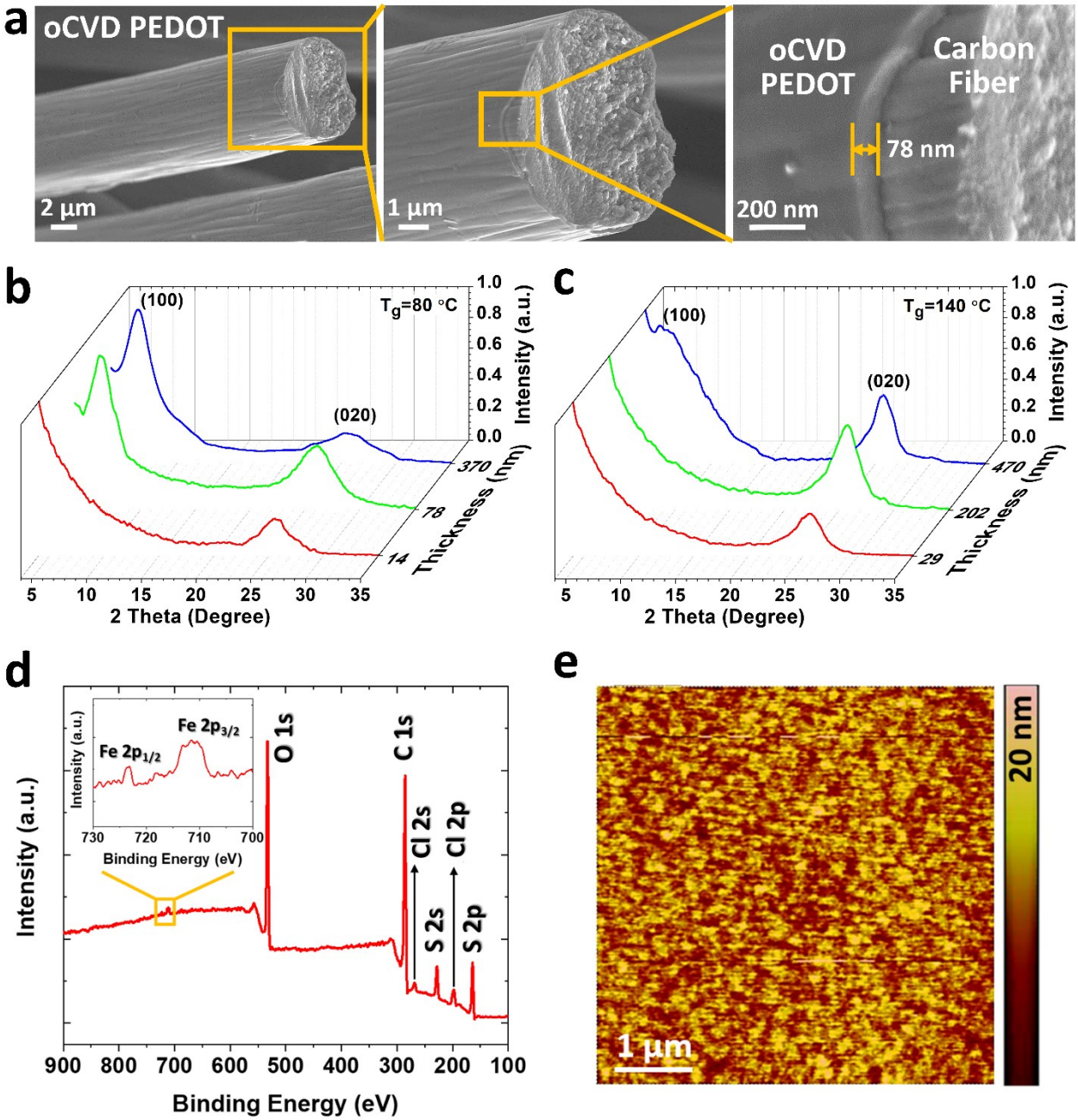

Figure 2. Structural characteristics of oCVD PEDOT film. (a) Cross-sectional SEM image of oCVD PEDOT coated carbon fiber grown at the deposition temperature of 80 °C. The out-of-plane GIXRD θ–2θ diffraction patterns of as-deposited oCVD PEDOT at the fixed $VOCl_3$ vapor saturation ratio and different growth temperature of (b) 80 °C and (c) 140 °C. (d) The XPS analyses of oCVD PEDOT grown on graphene and exposed to the iron chloride electrolyte. The penetration of iron into the oCVD PEDOT film is evinced by peaks at ~ 724 eV ($Fe\ 2p_{1/2}$) and ~ 712 eV ($Fe\ 2p_{3/2}$) as shown

This article is protected by copyright. All rights reserved.

in the inset. (e) The height AFM image of PEDOT thin film grown at the deposition temperature of 80 °C with the thickness of ca. 78 nm.

Normally, face-on orientation correlates with the low energy barrier of intercrystallite charge transport and induces the high in-plane carrier mobility and electrical conductivity.[27,35,37] Typically, there is a trade-off between in-plane and out-of-plane electrical conductivity in conducting polymers and the sample with high in-plane conductivity exhibits low out-of-plane conductivity and vice versa.[29,35]

To better understand the role of the PEDOT film chemical composition on electrochemistry, X-ray photoelectron spectroscopy (XPS) analysis was performed on the oCVD PEDOT coated planar substrate of graphene after overnight exposure to the iron chloride electrolyte (**Figure 2**d), with actives concentration of 0.5 M at 50% state-of-charge (SoC) in 2 M HCl. To overcome the shadowing effects of carbon fibers, we deposited oCVD PEDOT onto ten monolayers of graphene (Figure S4) and XPS analysis was carried out on the coated graphene sample after exposure to the electrolyte. The iron penetration into the oCVD PEDOT thin film can be noted based on the appeared peaks with low intensities at ca. 712 eV and 724 eV, which are related to the Fe $2p_{3/2}$ and Fe $2p_{1/2}$, respectively. The elemental composition was estimated from the XPS spectra of pristine PEDOT (Figure S5) and exposed PEDOT film to the electrolyte (**Figure 2**d) and summarized in Table S3 (Supporting Information). In addition to the presence of iron, elemental analysis reveals that the ratio of chlorine/sulfur (Cl/S), an indication of doping level, slightly decreases from its initial as-grown value of 0.37 to 0.30 after exposing to the electrolyte.

The surface topography of the oCVD PEDOT film grown at the deposition temperature of 80 °C with the thickness of ca. 78 nm is evaluated by atomic force microscopy (AFM) and is depicted in **Figure 2**e. The extracted surface roughness of oCVD PEDOT thin film was ca. 2.1 nm. The wetting properties of planar oCVD PEDOT thin films were previously investigated and exhibited the advancing water contact angle (WCA) of 62° and receding WCA of 22°.[38] Generally, in PEDOT thin films, the WCA depends on the root mean square (rms) roughness and the morphology of the surface based on the Cassie-Baxter equation.[39] The series of PEDOT thin films with different thickness grown with the same oxidant by the oCVD method exhibited approximately the same rms values, suggesting that the wetting properties were similar for the coated electrodes in this study. The film surface smoothness is of importance for some applications, such as avoidance of unwanted current leakage from inter-electrode shorting within photovoltaics,[17] but is anticipated to be of less relevance to RFB applications.

A photograph of oCVD PEDOT coated carbon fibers that were directly integrated into the RFB is shown in **Figure 3**a. Cyclic voltammograms (CVs) were conducted in aqueous acidic electrolytes containing iron salts to qualitatively assess oCVD PEDOT coated electrode activity (**Figure 3**b-c). In all experiments, the working electrode consisted of either untreated AvCarb 1071 (pristine) or oCVD PEDOT-coated AvCarb 1071. The solution compositions in cyclic voltammetry and flow cell testing consisted of total active species concentration of 0.5 M with 50% state of charge (SoC) for electroactive compounds, while the concentration of the supporting electrolyte was 2 M. To examine the impact of supporting salt counter-anion on oCVD PEDOT-coated electrodes, electrolytes with either hydrochloric acid (HCl) or sulfuric acid (H_2SO_4) were employed. Redox peaks were evident in all CVs for coated electrodes in iron-based solutions, indicating that coated electrodes are electrochemically active in iron solution regardless of the counter-anion. We are cautious about drawing definite conclusions from CVs due to the complexity of interpreting results for complex,

This article is protected by copyright. All rights reserved.

porous materials during potentiodynamic measurements.[40-42] The redox potential for the CVs (**Figure 3**b-c) were consistently ca 0.435 V vs Ag/AgCl, consistent with prior art.[43]

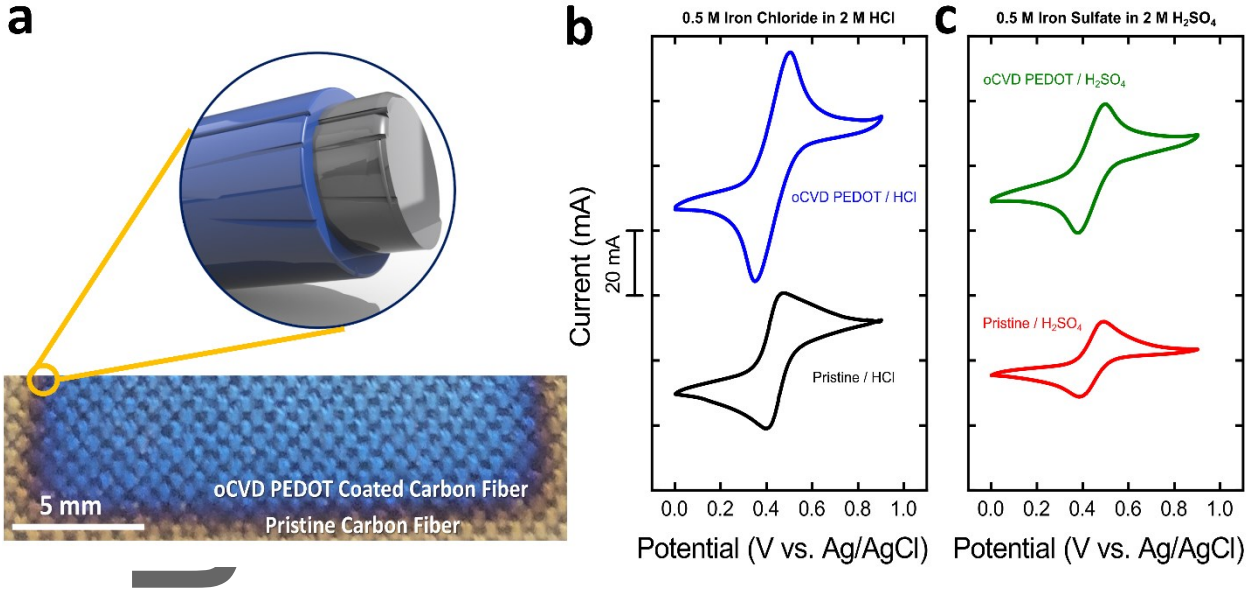

Figure 3. Ex-situ demonstration of oCVD PEDOT-coated electrodes in iron salts. (a) Photograph of oCVD PEDOT coated carbon fibers that were directly integrated into the RFB. Cyclic voltammograms (CVs) of oCVD PEDOT-coated and pristine electrodes in iron salts in aqueous acidic electrolyte solutions based on (b) HCl and (c) H_2SO_4, respectively. The CVs illustrate that PEDOT-coated electrodes are electrochemically reactive for iron-based electrolytes.

Based on the results from the CVs, we evaluate the performance of PEDOT-coated electrodes in iron-based solutions using a single-electrolyte flow cell configuration, quantifying resistive losses via electrochemical impedance spectroscopy (EIS) and cell polarization at steady-state conditions and 50% state-of-charge (SoC, schematic shown in **Figure 4**a).[43,44] In this setup, electrolyte is first oxidized at the positive electrode and then reduced at the negative electrode before re-circulation into the reservoir. The single-electrolyte flow cell configuration enables identification of individual contributions from ohmic, kinetic, and mass transport resistances in operation, without introducing additional extraneous variables that obfuscate the direct effect of the coating on electrode cell performance. The relative contribution of ohmic, kinetic, and mass transport resistances can be isolated by fitting an equivalent Randles-like circuit with bounded Warburg diffusion to Nyquist plots obtained using EIS. In this circuit, R_Ω corresponds to ohmics, R_{CT} to charge-transfer resistance, and R_{MT} extracted from bounded Warburg diffusion (W_δ) relates to mass-transfer resistance.[37,45]

Figure 4b shows a comparison of cell polarization for pristine and PEDOT coated electrodes with the best performance (T_g = 80 °C, 78 nm thickness) in iron chloride and iron sulfate electrolytes with an active species concentration of 0.5 M Fe(II)/Fe(III). In both electrolytes, coated electrodes demonstrate higher currents at similar applied overpotentials than uncoated electrodes, indicating lower resistance and higher power capabilities. The best-performing combination is the PEDOT-coated electrode in iron chloride, in part due to larger kinetic and mass transport resistances for iron sulfate compared to iron chloride.[46] However, at an applied overpotential of 350 mV, the relative increase in current for PEDOT-coated electrodes as compared to uncoated electrodes is greater in iron sulfate (~ 6.7×) than in iron chloride (~3.7×). The greater multiplicative enhancement of obtained current may be attributed to the improvement in crystallinity characteristics of PEDOT in H_2SO_4,

Author Manuscript

This article is protected by copyright. All rights reserved.

primarily an increase in the crystallite size. The obtained crystallite size in the a-axis direction (edge-on orientation) of pristine PEDOT and PEDOT treated with HCl and H_2SO_4 are 5.7, 6.0, and 7.6 nm, respectively (Figure S6, Supporting Information). The crystallinity enhancement of PEDOT is hypothesized to improve the kinetics of electron transfer rate by enabling better energetic overlapping the density of state (DOS) between PEDOT and redox-active species as predicted by the Marcus-Gerischer model.[31,35,47] The enhancement of electrochemical performance by improved crystallinity is also reported in poly(3-hexylthiophene) (P_3HT) due to the better DOS overlapping of the electrode and redox-active species.[48]

Encouragingly, we observe from fitted EIS data that the PEDOT coating reduces all forms of overpotential (**Figure 4**c,d) indicating that the conducting polymer film imparts multiple benefits. We attribute reduction in ohmics to result from better contact between current collector/electrode/membrane components due to polymeric interlayers. Improved surface area from better wetting[39] may partially explain kinetic enhancement, but the convolution of relevant factors pertaining to kinetics (i.e., available surface area, accessibility through PEDOT film, reactivity of carbon/PEDOT interface) are outside the scope of this initial report.

Of special pertinence, however, is the role of mass transport through the PEDOT film. While ohmic and kinetics are more difficult to tune, an understanding of ion transport through the nanolayer affords the possibility of using factors such as flow rate and electrolyte concentration to reducing mass transfer resistance in convection-enhanced cells. To this end, the performance of six electrodes at thicknesses of 14, 29, 78, 202, 370, and 470 nm was evaluated in the single-electrolyte flow cell in iron chloride (Figure S7). In our experimental setup, the highest currents were observed with a thickness of 78 nm, although shifts in performance across the film thicknesses were marginal relative to improvements over the pristine electrode. We note that the optimal coating thickness for highest power output will depend on system level factors such as operating flow rate, reactor configuration, and flow channel; furthermore, the optimal thickness is dependent on the desired electrochemical application and film material properties. The best-performing 78 nm thick semi-crystalline PEDOT film, grown at the deposition temperature of 80 °C, contains both edge-on (ca. 8.1%) and face-on (ca. 91.9%) orientations (Table S2). It is postulated that the presence of edge-on orientation, with sufficient electrical conductivity, is favorable for electrochemical applications and for facilitating ion transport.[30,31] Thus, the better electrochemical performance of 78 nm thick semi-crystalline PEDOT film grown at 80 °C can be attributed to the higher preferential edge-on orientation in that sample compared to its counterparts grown at 140 °C as well as those samples grown at 80 °C with the lower thickness. In addition to the preferential orientation, the thickness limit is another important parameter that needs to be considered. As mentioned earlier, conductive polymers are ionically permeable, and the upper thickness limit needs to be considered for enhanced ionic permeability characteristics of conducting polymers such as PEDOT. Xu et al.[16] also reported the presence of a thickness limit in PEDOT thin films for electrochemical applications. Specifically, they reported an optimal oCVD PEDOT film thickness of 20 nm to obtain the best performance in layered lithium transition metal oxide cathodes such as $LiNi_{1/3}Co_{1/3}Mn_{1/3}O_2$ (NCM111).

Magnitudes of mass transport overpotential at flow rates of 5 mL min^{-1} and 15 mL min^{-1} are detailed in **Figure 4**e. Mass transport overpotential as a function of thickness is discontinuous at ~50 nm, which we tentatively ascribe to a transition from lower to higher-dimensional transport regimes.[28] Above 50 nm thickness, mass transport increases linearly, suggesting thicker PEDOT layers increase resistance to active species diffusion to a buried reactive carbon/PEDOT interface.

This article is protected by copyright. All rights reserved.

Mass transport is also convection dependent, as the higher flow rate exhibits the same trend as the lower flow rate, but with lower overpotential. Therefore, both convection and thickness affect mass transport, operating simultaneously during flow cell operation. **Figure 4**e suggests that partitioning of reactive iron species between the electrolyte and PEDOT film occurs, in which $Fe^{2+/3+}$ becomes entrapped in the PEDOT film, reducing the effective boundary layer required for the redox actives to diffuse to the reactive carbon interface. In this scenario, we hypothesize convection influences total mass transport by homogenizing the concentration of the bulk electrolyte, forming a boundary layer as actives diffuse from the bulk electrolyte to the PEDOT film, thus influencing the partitioning and concentration of iron actives at the electrolyte/PEDOT surface.

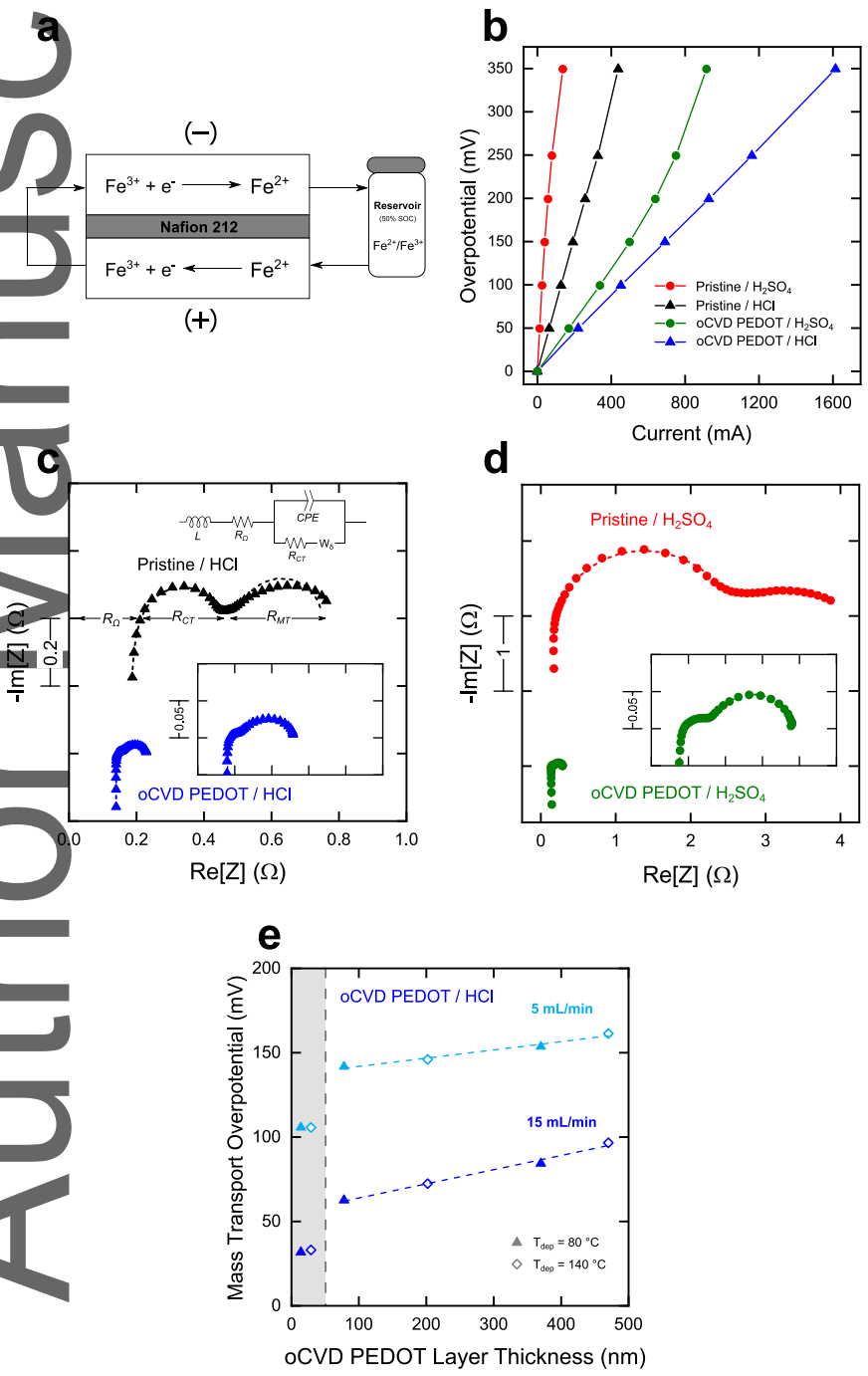

Author Manuscript

This article is protected by copyright. All rights reserved.

Figure 4. PEDOT-coated electrodes improve performance in iron-based electrolytes. (a) Schematic of single-electrolyte flow cell configuration, using Fe^{2+}/Fe^{3+} as a model redox couple, for evaluating electrode performance. (b) Cell polarization data for 50% state-of-charge (0.25 M Fe^{2+} / 0.25 M Fe^{3+}) at a flow rate of 15 mL min^{-1}. Nyquist plots obtained using EIS for oCVD PEDOT and pristine carbon fiber in (c) HCl supporting salt and (d) H_2SO_4 supporting salt, with the same conditions as (b). The equivalent circuit used to fit the impedance data is shown in (c). Insets are closer views of the PEDOT Nyquist plots. (e) Mass transport overpotential determined from the equivalent circuit as a function of PEDOT layer thickness at two different flow rates (5 and 15 mL min^{-1}).

Insights into the structure of coated carbon fiber exposed to the iron-based electrolyte reveals that the durable and stable nature of the conformal oCVD PEDOT film is maintained after electrochemical tests within the flow cell (**Figure 5**a). There was no observed delamination and the integrity of the oCVD PEDOT film is also maintained after electrochemical reactions and can be directly observed from the electrode cross-section energy dispersive spectroscopy (EDS) mapping of the oxygen element (**Figure 5**b) and other elemental components of PEDOT (Figure S8, Supporting Information). The trace of iron can be noted in the elemental EDS mapping (**Figure 5**c), which is consistent with obtained XPS results (**Figure 2**d), and further support our earlier hypotheses on the penetration of iron cations into the nanometric film. To further examine mass transport behavior through the film, polarization and EIS for the relatively thicker 202 nm PEDOT-coated electrode was evaluated across a range of iron chloride electrolyte concentrations (0.02, 0.5, and 1.0 M Fe^{2+}/Fe^{3+}) and compared to the uncoated electrode, shown in **Figure 5**. For uncoated electrodes, the resistance distribution (**Figure 5**e) based on equivalent circuit fits to Nyquist plots (**Figure 5**d) shows a consistent reduction in kinetic and mass transport resistance with increasing concentration, in agreement with prior art.[49,50] Interestingly, in PEDOT-coated electrodes, mass transport resistance reduces significantly from 0.02 M to 0.5 M, but experiences diminishing returns from 0.5 M to 1.0 M, despite similar ohmic and kinetic resistances at all concentrations (**Figures 5**h and g). Cell polarization of coated electrodes (**Figure 5**i) shows marked performance improvement between 0.02 and 0.5 M concentrations, while 0.5 and 1.0 M are nearly identical. This observation appears to indicate that, in this concentration range, the overall mass transfer coefficient is independent of iron concentration in the flowing electrolyte as the iron concentration partitioned into the PEDOT film is at saturation. Surprisingly, despite the PEDOT film acting as a second resistance to mass transport, overall redox rate increases. We hypothesize that preferential segregation of iron into the PEDOT as observed by XPS after film exposure to the electrolyte still reduces effective iron concentration gradients at the electrode surface, thus lowering overall mass transport resistance. To conclude the discussion on transport, the results suggest that two modes of mass transport resistance act for the coated electrodes: (1) diffusion from the bulk electrolyte to the PEDOT surface, which is not significantly affected by the presence of the coating, and (2) assisted diffusion unique to the oCVD PEDOT coatings whereby iron active species partitioning into the nanometric film improve overall mass transfer. This phenomenon will be explored in detail in a subsequent publication.

This article is protected by copyright. All rights reserved.

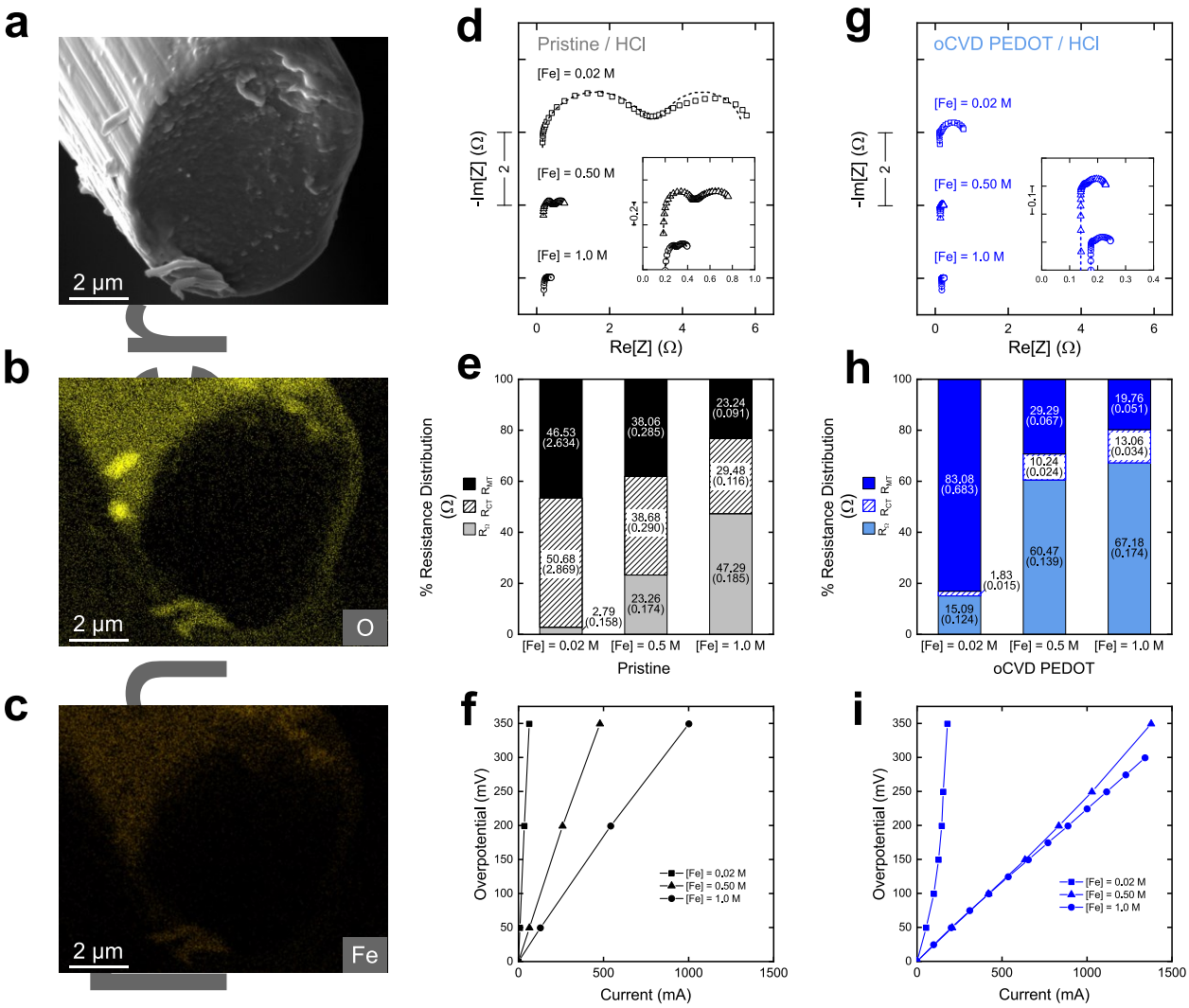

Figure 5. Mass-transport limitation through PEDOT film. (a) SEM cross-section of oCVD PEDOT-coated carbon fiber after exposure to electrolyte. The electrochemical stability of oCVD PEDOT can be noted. EDS mapping of (b) oxygen and (c) iron. Nyquist plots from electrochemical impedance spectroscopy of (d) pristine carbon fiber and (g) 202 nm oCVD PEDOT-coated electrode in 0.02, 0.50, and 1.0 M iron chloride. Distribution of ohmic (R_Ω), charge-transfer (R_{CT}), and mass-transport (R_{MT}) resistances based on equivalent circuit fits of Nyquist plots for (e) pristine and (h) oCVD PEDOT-coated. Cell polarization at concentrations of 0.02, 0.50, and 1.0 M iron chloride for (f) pristine and (i) oCVD PEDOT-coated.

To investigate the longevity of the PEDOT coating, a symmetric cell galvanostatic cycling experiment was performed in iron chloride electrolyte over the course of ~2.9 days (**Figure 6**). The cells were cycled for five times at current densities of 50, 75, 100, 125, 150, and again at 50 mA cm^{-2} to assess changes in performance after higher current density cycling. **Figure 6a,b** reveal that PEDOT-coated electrodes cycle longer than pristine electrodes due to fewer overpotential losses. Nyquist plots before and after cycling are similar in appearance and overall resistance, demonstrating that the PEDOT-coated electrode are stable (**Figure 6c**) without any delamination issue as shown in Figure 5-a-c and Figure S8. Furthermore, the discharge capacity exceeds 80% even after several days

This article is protected by copyright. All rights reserved.

of cycling, exceeding that of the pristine (**Figure 6d**). Therefore, we show that benefits from using PEDOT-coatings on electrodes are electrochemically and mechanically durable over longer durations.

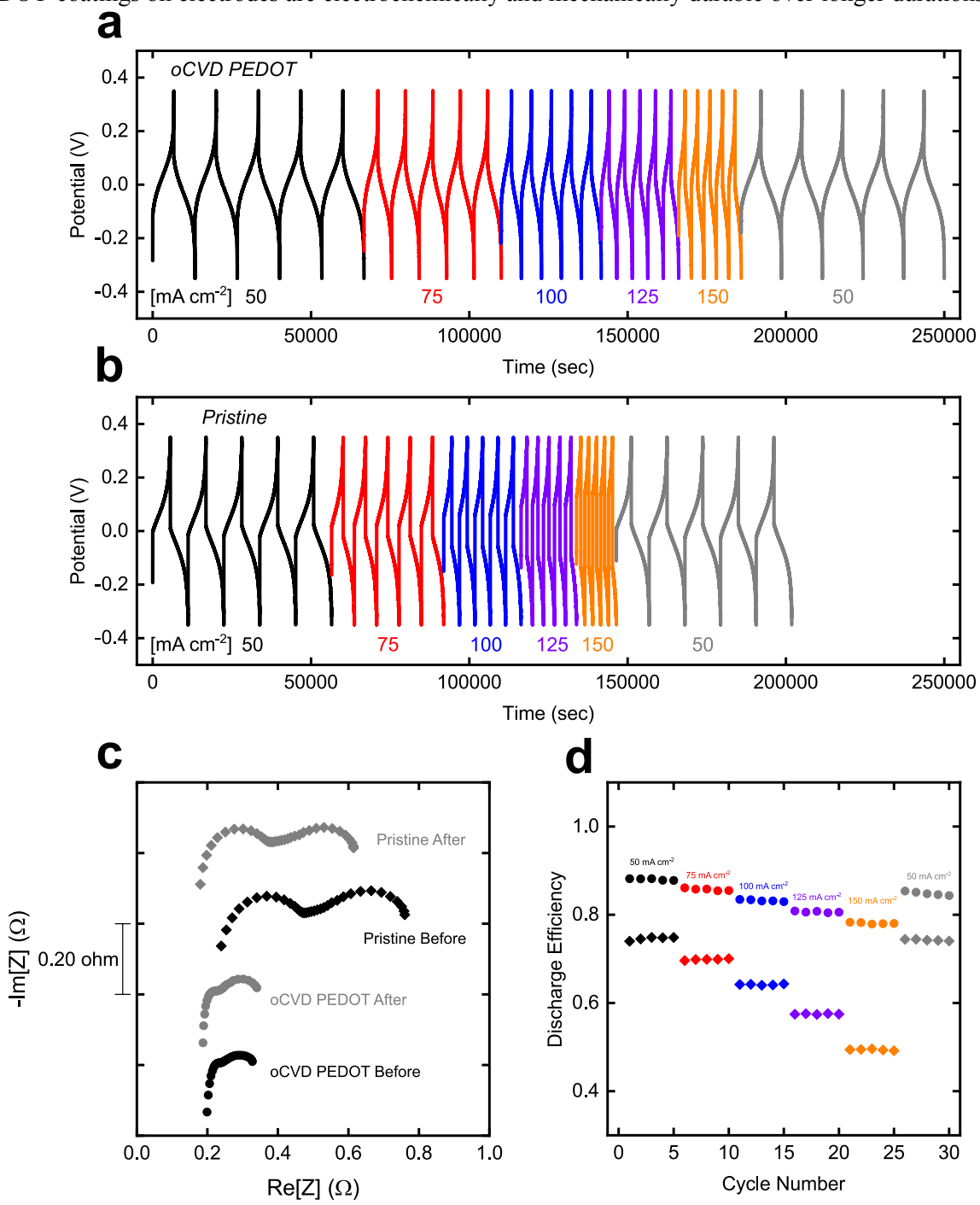

Figure 6. PEDOT films remain stable and are durable after cycling for several days. Symmetric cell galvanostatic cycling at several current densities in iron chloride of (a) oCVD PEDOT coated electrodes and (b) pristine electrodes. (c) Impedance spectroscopy before and after cycling for both oCVD PEDOT and pristine electrodes. (d) Discharge efficiency versus cycle number using theoretical discharge capacity as a basis.

Conclusion

This article is protected by copyright. All rights reserved.

In summary, we demonstrate that ultraconformal semi-crystalline oCVD PEDOT coated carbon fiber electrodes are promising for RFBs. PEDOT-coated electrodes enhanced maximum current density by ~6.7× in iron sulfate, and ~3.7× in iron-chloride, due to a reduction in ohmic, kinetic, and mass transport overpotentials. To examine the transport of iron through the PEDOT film, we tested PEDOT films of varying thickness, under conditions with different electrolyte flow rates and concentrations, finding that mass transport overpotential varies as a function of thickness and convection. The dependence on both factors suggests mass transport limitation has two components in series, the first consisting of transport through the boundary layer of the electrolyte and the second consisting of transport through the oCVD PEDOT layer. An optimal oCVD PEDOT thickness of 78 nm at a 15 mL min^{-1} flow rate was identified. The demonstration of oCVD PEDOT coated electrodes enhancing performance presents future opportunities for the advanced surface engineering of porous materials in RFBs to mediate desired electrochemistry.

Acknowledgments

We acknowledge the support from MIT's Center for Materials Science and Engineering Shared Experimental Facilities, supported in part by the MRSEC Program of the National Science Foundation under award number DMR1419807 and the Institute for Soldier Nanotechnologies, sponsored by the U.S. Army Research Office. Research by C.T.W., A.F.C., K.V.G, Y.M.C., and F.R.B. was supported by the Joint Center for Energy Storage Research (JCESR), an Energy Innovation Hub funded by the U.S. Department of Energy, Office of Science, Basic Energy Sciences. C.T.W. acknowledges a graduate fellowship through the National Science Foundation Graduate Research Fellowship Program under Grant No. 1122374. K.V.G. acknowledges additional funding from the National Science Foundation Graduate Research Fellowship under grant no. 1122374. Any opinions, findings, and conclusions or recommendations expressed in this material are those of the authors and do not necessarily reflect the views of the National Science Foundation. A.F.C. acknowledges the Swiss National Science Foundation for funding his postdoctoral fellowship (Gran No. P2EZP2_172183).

CRediT authorship contribution statement

Meysam Heydari Gharahcheshmeh: Conceptualization, Methodology, Validation, Formal analysis, Investigation, Data Curation, Writing – Original Draft, Writing – Review & Editing, Visualization. **Charles Tai-Chieh Wan:** Conceptualization, Methodology, Validation, Formal analysis, Investigation, Data Curation, Writing – Original Draft, Writing – Review & Editing, Visualization. **Yasser Ashraf Gandomi:** Validation, Formal analysis, Investigation, Data Curation, Writing – Review & Editing. **Katharine Greco:** Validation, Investigation, Writing – Review & Editing. **Antoni Forner-Cuenca:** Conceptualization, Methodology, Writing – Review & Editing. **Yet-Ming Chiang:** Resources. **Fikile R. Brushett:** Conceptualization, Resources, Writing – Original Draft, Writing – Review & Editing, Supervision. **Karen K. Gleason:** Conceptualization, Resources, Writing – Original Draft, Writing – Review & Editing, Supervision.

References

This article is protected by copyright. All rights reserved.

[1] A. Z. Weber, M. M. Mench, J. P. Meyers, P. N. Ross, J. T. Gostick, Q. Liu, *J. Appl. Electrochem.* **2011**, 41, 1137.
[2] M. L. Perry, A. Z. Weber, *J. Electrochem. Soc.* **2016**, 163, A5064.
[3] W. Wang, Q. Luo, B. Li, X. Wei, L. Li, Z. Yang, *Adv. Funct. Mater.* **2013**, 23, 970.
[4] M. Skyllas-Kazacos, M. H. Chakrabarti, S. A. Hajimolana, F. S. Mjalli, M. Saleem, *J. Electrochem. Soc.* **2011**, 158, R55.
[5] C. Zhang, L. Zhang, Y. Ding, S. Peng, X. Guo, Y. Zhao, G. He, G. Yu, *Energy Storage Mater.* **2018**, 15, 324.
[6] K. J. Kim, M. S. Park, Y. J. Kim, J. H. Kim, S. X. Dou, M. Skyllas-Kazacos, *J. Mater. Chem. A.* **2015**, 3, 16913.
[7] A. Forner-Cuenca, F. R. Brushett. *Curr. Opin. Electrochem*. **2019**, 18, 113.
[8] K. V. Greco, A. Forner-Cuenca, A. Mularczyk, J. Eller, F. R. Brushett, *ACS Appl. Mater. Interfaces*. **2018**, 10, 44430.
[9] B. Sun, M. Skyllas-Kazacos, *Electrochim. Acta.* **1992**, 37, 1253.
[10] J. Kim, H. Lim, J. Y. Jyoung, E. S. Lee, J. S. Yi, D. Lee, *Carbon* **2017**, 111, 592.
[11] D. Kil, H. J. Lee, S. Park, S. Kim, H. Kim, *J. Electrochem. Soc.* **2017**, 164, A3011.
[12] W. Zhang, J. Xi, Z. Li, H. Zhou, L. Liu, Z. Wu, X. Qiu, *Electrochim. Acta*. **2013**, 89, 429.
[13] Y. Men, T. Sun, *Int J Electrochem Sci.* **2012**, 7, 7.
[14] B. Sun, M. Skyllas-Kazacos, *Electrochimi. Acta.* **1992**, 37, 2459.
[15] Y. Zhou, X. Wang, L. Acauan, E. Kalfon-Cohen, X. Ni, Y. Stein, K. K. Gleason, B. L. Wardle, *Adv. Mater.* **2019**, 31, 1901916.
[16] G. Liang Xu, Q. Liu, K. K. S. Lau, Y. Liu, X. Liu, H. Gao, X. Zhou, M. Zhuang, Y. Ren, J. Li, M. Shao, M. Ouyang, F. Pan, Z. Chen, K. Amine, G. Chen, *Nat. Energy* **2019**, 4, 484.
[17] M. Heydari Gharahcheshmeh, K. K. Gleason, *Adv. Mater. Interfaces* **2019**, 6, 1801564.
[18] K. K. Gleason, *J. Vac. Sci. Technol. A*, **2020**, 38, 00452.
[19] D. Bilger, S. Z. Homayounfar, T. L. Andrew, *J. Mater. Chem. C.* **2019**, 7, 7159.
[20] S. Kaviani, M. M. Ghaleni, E. Tavakoli, S. Nejati, *ACS Appl. Polym. Mater*. **2019**, 1, 552.
[21] D. Farka, H. Coskun, J. Gasiorowski, C. Cobet, K. Hingerl, L. M. Uiberlacker, S. Hild, T. Greunz, D. Stifter, N. S. Sariciftci, R. Menon, W. Schoefberger, C. C. Mardare, A. W. Hassel, C. Schwarzinger, M. C. Scharber, P. Stadler, *Adv. Electron. Mater.* **2017**, 3, 1700050.
[22] M. Heydari Gharahcheshmeh, K. K. Gleason, *Adv. Mater. Interfaces* **2019**, 6, 1970016.
[23] L. Su, P. M. Smith, P. Anand, B. Reeja-Jayan, *ACS Appl. Mater. Interfaces* **2018**, 10, 27063.
[24] H. Goktas, X. Wang, N. D. Boscher, S. Torosian, K. K. Gleason, *J. Mater. Chem. C* **2016**, 4, 3403.
[25] M. N. Gueye, A. Carella, J. Faure-Vincent, R. Demadrille, J. P. Simonato, *Prog. Mater. Sci.* **2020**, 108, 100616.
[26] P. Kovacik, G. d. Hierro, W. Livernois, K. K. Gleason, *Mater. Horiz.* **2015**, 2, 221.
[27] M. Heydari Gharahcheshmeh, M. M. Tavakoli, E. F. Gleason, M. T. Robinson, J. Kong, Karen K. Gleason, *Sci. Adv.* **2019**, 5, eaay0414.
[28] A. Ugur, F. Katmis, M. Li, L. Wu, Y. Zhu, K. K. Varanasi, K. K. Gleason, *Adv Mater.* **2015**, *27*, 4604.
[29] X. Wang, X. Zhang, L. Sun, D. Lee, S. Lee, M. Wang, J. Zhao, Y. Shao-Horn, M. Dinca, T. Palacios, K. K. Gleason, *Sci. Adv.* **2018**, 4, eaat5780.
[30] P. Moni, J. Lau, A. C. Mohr, T. C. Lin, S. H. Tolbert, B. Dunn, K. K. Gleason, *ACS Appl. Energy Mater.* **2018**, 1, 7093.
[31] S. P. Arnold, J. K. Harris, B. Neelamraju, M. Rudolph, E. L. Ratcliff, *Synth. Met.* **2019**, 253, 26.
[32] M. Coclite, R. M. Howden, D. C. Borrelli, C. D. Petruczok, R. Yang, J. L. Yague, A. Ugur, N. Chen, S. Lee, W. J. Jo, A. Liu, X. Wang, K. K. Gleason, *Adv. Mater.* **2013**, 25, 5392.
[33] S. Vaddiraju, H. Cebeci, K. K. Gleason, B. L. Wardle, *ACS Appl. Mater. Interfaces*, **2009**, 1, 2565.
[34] K. K. Gleason, *Nat. Rev. Phys*. **2020**, 2, 347.
[35] M. Heydari Gharahcheshmeh, K. K. Gleason, *Materials Today Advances*, **2020**, 8, 1000862.

This article is protected by copyright. All rights reserved.

Author Manuscript

[36] L. E. Alexander, in X-Ray Diffraction Methods in Polymer Science (Wiley Series on the Science and Technology of Materials), John Wiley & Sons Inc., **1969**.
[37] S. D. Kang, G. J. Snyder, *Nat. Mater.* **2017**, 16, 252.
[38] M. Wang, P. Kovacik, K. K. Gleason, *Langmuir,* **2017**, 33, 10623.
[39] S. G. Im, D. Kusters, W. Choi, S.H. Baxamusa, M. C. M. van de Sanden, K. K. Gleason, *ACS nano*, **2008**, 2 (9), 1959.
[40] I. Streeter, G. G. Wildgoose, L. Shao, R. G. Compton, *Sens. Actuators B Chem.* **2008**, 133, 462.
[41] C. Punckt, M. A. Pope, I. A. Aksay, *J. Phys. Chem. C.* **2013**, 117, 16076.
[42] J. Friedl, U. Stimming, *Electrochimica Acta*. **2017**, 227, 235.
[43] A. Forner-Cuenca, E. E. Penn, A. M. Oliveira, F. R. Brushett, *J. Electrochem. Soc.* **2019**, 166, A2230.
[44] R. M. Darling, M. L. Perry, *J. Electrochem. Soc.* **2014**, 161, A1381.
[45] J. D. Milshtein, J. L. Barton, R. M. Darling, F. R. Brushett, *J. Power Sources*, **2016**, 327, 151-159.
[46] M. Stulikova, F. Vydra, *J. Electroanal. Chem.* **1972**, 38, 349
[47] M. Rudolph, E. L. Ratcliff, *Nat. Commun*. **2017**, 8, 1048.
[48] B. Neelamraju, M. Rudolph, E. L. Ratcliff, *J. Phys. Chem. C*. **2018**, 122, 21210.
[49] J. D. Milshtein, K. M. Tenny, J. L. Barton, J. Drake, R. M. Darling, F. R. Brushett, *J. Electrochem. Soc.* **2017**, 164, E3265.
[50] M. Pezeshki, R. L.Sacci, F. M.Delnick, D. S.Aaron, M. M. Mench, *Electrochim. Acta*, **2017**, 229, 261.

Author Manuscript

This article is protected by copyright. All rights reserved.